Data-driven modelling of the FRC network for studying the fluid flow in the conduit system

Rostislav Savinkov[a,b], Alexey Kislitsyn[a,b], Daniel J. Watson[c], Raoul van Loon[c], Igor Sazonov[c], Mario Novkovic[d], Lucas Onder[d], Gennady Bocharov[a,*]

[a] *Institute of Numerical Mathematics of the RAS, Moscow, Russian Federation*
[b] *Lomonosov Moscow State University, Moscow, Russian Federation*
[c] *College of Engineering, Swansea University, Swansea, Wales, U.K.*
[d] *Institute of Immunobiology, Kantonsspital St. Gallen, St. Gallen, Switzerland*

Abstract

The human immune system is characterized by enormous cellular and anatomical complexity. Lymph nodes (the key centers of immune reactivity) are organized into distinct structural and functional modules including the T-cell zone, fibroblastic reticular cell (FRC) network and the conduit system. A thorough understanding of the modular organization is a prerequisite for lymphoid organ tissue-engineering. Because of the inherent complexity, it requires the development of computational models to capture the lymph node architecture and functional organization. We present a computational method to model the geometry of the FRC network. It differs from the text-colorredblood vascular network image-based reconstruction approaches as it develops the parameterized geometric model using the real statistics of the node degree and the edge length distributions.

The FRC network model is then used to analyze the fluid flow through the network. A first observation is that the pressure gradient is approximately linear, which suggests homogeneity of the network. Furthermore, calculated permeability values ($\approx\ 0.0033\ \mu m^2$) show the generated network is isotropic, while investigating random variations of pipe radii (with a given mean and STD) shows a significant effect on the permeability. This framework can now be further explored to systematically correlate fundamental characteristics of the FRC conduit system to more global material properties such as

*Corresponding author. E-mail address: bocharov@m.inm.ras.ru

permeability.

Keywords: Lymph node engineering, fibroblastic reticular cell, conduit system, complex vascular network, artificial networks, fluid flow

1. Introduction

The human immune system is characterized by enormous cellular and anatomical complexity that is required from a systems point of view to provide a robust protection against a broad range of pathogens and tumors. Models based on immune system principles have been increasingly developed and applied in the fields of science and engineering [9].

The immune system is a subject of great research interest because it performs powerful information processing in a highly parallel and distributed fashion resulting in its ability of recognition, learning, feature extraction, distributed detection, dynamic protection, etc. One of the key issues underlying the above properties is the transport of the information bearing molecules (e.g., antigens, cytokines, chemokines) or cells from the infected tissues to the organs of the immune system with lymph flow. The transport processes can be subdivided into two categories: the lymph flow from interstitial tissues to the draining lymph nodes (LNs) via the collecting network of lymphatic capillaries, lymphangions and vessels to thoracic duct and the lymph transport through lymph nodes in which the information processing governing the immune responses takes place. As it was shown recently, about 90 % of the lymph entering the lymph node takes a peripheral path to leave the node via efferent lymphatic vessels. The remaining 10 % of the lymph gains entry to the internal part of the lymph node, which is densely packed with immune cells of various types, e.g. antigen presenting cells (APCs), T-cells, B-cells. This occurs via the reticular network, which comprises reticular fibers, related extracellular matrix components, and associated fibroblastic reticular cells (FRCs) constituting a conduit system for bulk flow delivery of soluble molecules to distinct sites in the paracortex, particularly the high endothelial venules [11, 12, 30]. This network is a multifunctional three-dimensional infrastructure that facilitates encounters of cells with other cells and factors necessary for effective and efficient immune surveillance. Given the importance of biological mediators in regulating immune responses, it is essential to understand the quantitative parameters of the lymph flow through the conduit system in health and disease as this directly impacts the spatial and

temporal aspects of information delivery to the reactive parts of the lymph node. The mathematical modelling of the conduit system and the fluid flow through the network will serve to replace a descriptive characterization of the transport system with a quantitative framework.

LNs are the key centers of immune reactivity. Some pathologies are associated with the destruction of lymphoid tissue organization, e.g. the infection with human immunodeficiency virus [14] or melanoma [31]. One plausible approach to reconstitution of the LN functionality is based on activation of the natural remodelling processes, including the lymphoid tissue inducer (LTi) cells [20]. Another possibility is based on bio-engineering of an artificial LN [6, 25]. Both present a formidable challenge due to the high level of complexity resulting from the highly organized stromal and lymphoid structures. LNs are compartmentalized into distinct structural and functional modules such as the subcapsular sinus, trabecular- and medullar sinuses, B-cell follicles, medulla, blood vasculature including high endothelial venules (HEVs), T-cell zone, fibroblastic reticular cell (FRC) network and the conduit system [21, 30, 27]. A thorough understanding of the modular organization is a prerequisite for lymphoid organ tissue-engineering. Because of inherent complexity, the development of computational models capable of capturing the LN architecture and functional organization is required. The LN scaffold and lymph transport through the conduit system ensheathed by the FRC network appear to be most difficult to describe computationally. Indeed, the latest studies of the fluid flow in LNs [13, 7] do not consider the FRC network.

The computational reconstruction of 3D morphology of lymphoid tissues is based on a direct use of the imaging data generated by various techniques ranging in their resolution. The broad availability of various imaging techniques has enabled the spatial characterization of LN structures [24, 32]. A mesoscopic imaging represented by selective plane illumination microscopy (SPIM) and optical projection tomography (OPT) [22] allow visualization of major LN structures, such as B-cell follicles, HEVs and the subcapsular sinus. However, more complex LN structures, such as the FRC network enwrapping the conduit system, require application of higher resolution techniques, e.g., confocal microscopy, to generate information on the structural properties of the FRC network [15]. Existing approaches for generation of LN vascular networks can be subdivided into two major categories: the reconstruction- [10] and the modelling-based algorithms [29]. Because of an extremely variable appearance of the FRC network, the reconstruction-based algorithms are not

applicable yet. Therefore, the geometric modelling approach is currently the only feasible solution to develop computational models of the FRC network in parameterized forms suitable for further application studies of transport phenomena in the LN.

In the following parts of Section 1 we provide an overview of existing approaches to model vascular networks and give the relevant details of the experimental data generation. Then we present an efficient computational algorithm to to generate 3D network model using experimental data on the statistics of the node degree- and edge length distributions the FRCs network both as an idealized topological structure and as real solid object model in Sections 2 and 3. The generated FRC network is finally used to study the fluid flow through lymph node conduits in Section 4.

1.1. Approaches to vascular branching networ generation

Numerous existing approaches to the generation of vascular networks deal with the blood vasculature. Most of the approaches consider degree one (endpoints) and degree-three nodes (bifurcations) of the vessels to build up a graph representation of the networks. Three different methodologies are employed in these studies: (i) a skeleton-based graph reconstruction from vascular segmentations [4, 8]; (ii) a biophysical modelling of the morphogenesis with convection-reaction-diffusion systems [23] [29], and (iii) using ad hoc assumptions about the optimality of the network topology with respect to some potential energy of the interactions between the nodes [16]. Whereas theoretically it is possible to adapt the above approaches for the FRC network generation, currently to our knowledge no algorithms for modelling the FRC network from real spatial data exist. In this study we propose such an algorithm to model the FRC network topology and geometry based on direct use of quantitative real data on the node degree- and edge length distributions.

Computational modelling algorithms aim to generate blood vascular networks using the information on the degree- and the edge length distribution as well as the spatial embedding of the network. The modelling algorithms can be based on fractal trees, i.e. a binary tree approximating the vascular network structure. An example is provided by a binary tree approximating the brain vascular network [2]. A more elaborate algorithm considers the fractal tree constructed using the level set distance function [3]. Other examples of the fractal tree network construction are reviewed in [28]. A specific approach based on spring embedders and force directed graph drawing

algorithms was formulated in [16]. The graph is represented as a network of connected vertices, positioned according to the action of springs, iteratively pulling the nodes to attain an optimal configuration corresponding to the potential energy minimum of the system. The major advantage of the network graph generation using the fractal tree approach is due to the simplicity of its implementation and analysis. However, the fractal approach is not efficient in the case of the FRC network because of its high degree of connectivity. The algorithm based on spring embedders is potentially applicable for usage in FRC network generation but is likely to be computationally very demanding. In comparison to the force-directed methods, the FRC network modelling algorithm presented in this paper, allows one to move nodes and connections (edges) to achieve the target distances between them and to split the connections and curve edges for allocating the positions of vessels in a way which does not necessarily lead to a symmetry.

1.2. Data generation for the algorithm

The computational algorithm for the generation of the FRC network data has been previously developed [15]. Briefly, $Ccl19-CrexR26-eyfp$ reporter mice [17] were used to target FRCs specifically in murine inguinal LNs. Z-stack images (approximately 300x300x30 μm) of the T cell zone FRC network were acquired by confocal microscopy and quantitative morphological analysis [18] was performed on single FRCs in Imaris (Bitplane). The number of protrusions were calculated per FRC indicated as the number of edges per node in Figure 1. The lengths of the protrusion segments (edge length in Figure 1) were calculated using Filament Tracer in Imaris. The imaging-based real geometry FRC statistics were implemented in the computational algorithm for the FRC network construction, which is described in detail in the next section. Animal experiments were performed in accordance with federal and cantonal guidelines (Tierschutzgesetz) under the permission numbers $SG13/05$ and $SG13/04$ following review and approval by the Veterinary Office of the Canton of St. Gallen.

Figure 1 below presents the spatially realistic FRC network data (A) on edge length and (B) node degree distributions, , respectively.

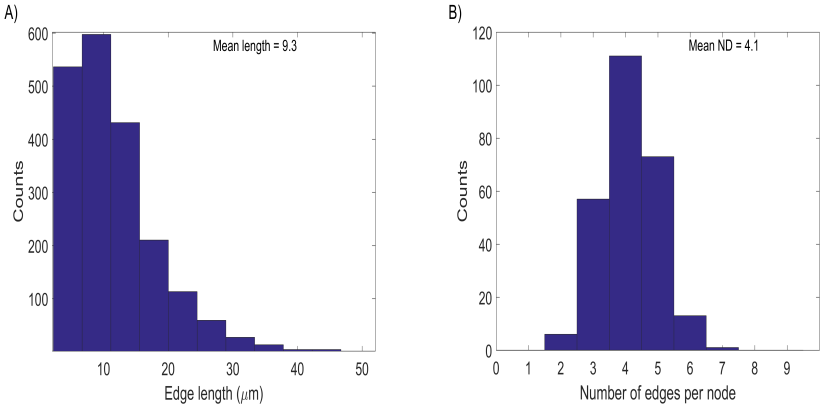

Figure 1: Real geometry FRC network statistics: A) the distribution of the edge lengths and B) the distribution of the number of links per node, Mean ND is the average number of links per node (degree). Data represent topological analyses of the T cell zone FRC network data sampled from 3 mice.

2. FRC network generating algorithm

2.1. Description of the algorithm

Two 1D arrays, $\{\mathbf{d}_n\}$ and $\{\mathbf{L}_e\}$, are generated of random values distributed in accordance with the experimental FRC histograms of nodal indices (node degree) and conduits lengths, respectively. An $N \times N \times N$ grid of nodes is generated with $N = 11$ and the grid step $h = 5$ μm. A nodal index chosen randomly from the $\{\mathbf{d}_n\}$ array is assigned to every node in the grid.

Considering one-by-one every node n, the possibility is checked to establish a new link between node n and another node randomly taken from its 26-neighbouring. A link can be established if the current nodal indices of both nodes are less than the respective assigned nodal indices. In this case the link is stored as a graph edge, and a target length is assigned to it by randomly taking a value from the $\{\mathbf{L}_e\}$ array. At the end of this stage (requiring $O(N_n = N^3)$ operations) we obtain a graph with nodes located on a regular rectangular grid with appropriately distributed nodal indices. Note that the edge lengths in this graph will be h, $\sqrt{2}h$ or $\sqrt{3}h$, which generally does not coincide with the assigned edge lengths.

Hence, the next stage is to perturb the nodes without changing the graph topology such that the edge lengths become as close as possible to the length

values previously assigned from $\{\mathbf{L}_e\}$. The total number of operations in such an algorithm is estimated to be $O(N_n^2)$. To make it faster, i.e. $O(N_n)$, we split the total domain by a set of $S\times S\times S$ cubic subdomains with $S = 10$ μm and associate every node with the subdomain containing that node. Then we compose the attraction/repulsion forces moving the contiguous nodes to the target distance whilst introducing repulsive forces between node n and all the non-contiguous nodes belonging to the same or adjacent subdomains.

The second stage is implemented via the following iterations. For every node n with physical coordinates $\mathbf{P}_n = \{x_n, y_n, z_n\}$ from a given subdomain find the set of all contiguous nodes $\mathcal{N}_n$ and a set of all the nodes belonging to this or adjacent subdomain $\mathcal{K}_n$ (excluding node n). Then the new position of node n is calculated as

$$\mathbf{P}_n^{\text{new}} = \mathbf{P}_n + \Delta\mathbf{P}_n \text{ where } \Delta\mathbf{P}_n = \sum_{m\in\mathcal{N}_n} \Delta\mathbf{P}_{nm} + \sum_{k\in\mathcal{K}_n\setminus\mathcal{N}_n} \Delta\mathbf{P}_{nk}$$

$$\Delta\mathbf{P}_{nm} = \frac{\mathbf{P}_m - \mathbf{P}_n}{2L_{nm}}(L_{nm} - L_{nm}^t)$$

$$\Delta\mathbf{P}_{nk} = \frac{\mathbf{P}_k - \mathbf{P}_n}{2L_{nk}}(L_{nk} - L^{\mathcal{K}}) \text{ if } L_{nk} < L^{\mathcal{K}} \text{ otherwise } 0.$$

Here $L_{nm} = \|\mathbf{P}_m - \mathbf{P}_n\|$ is the current Euclidian distance between the nodes, L_{nm}^t is the target distance between them (i.e. assigned from $\{\mathbf{L}_e\}$ to the given edge) and $L^{\mathcal{K}}$ is the minimal allowed distance for non-contiguous nodes. Our numerical simulation shows that $L^{\mathcal{K}} = 6.5$ μm is a good choice for obtaining a realistic graph.

After updating the position of the nodes, every node is again associated with a subdomain (typically it is the same subdomain or an adjacent one). This algorithm is repeated until the maximal displacement $\max_n |\Delta\mathbf{P}_n| < \varepsilon$ where ε is a prescribed value which determines the accuracy of targeting the edge lengths. We take $\varepsilon = 0.1$ in our simulation.

2.2. Pseudocode representation

Below the algorithm is specified as pseudocode.

Input: Regular cube with N^3 nodes array *node*. $NodeIndex$ is an array with randomly distributed nodal indexes generated using the experimental data. $EdgeTarget$ is an array with randomly distributed lengths of edges generated using the experimental data. $CONST_1$

and $CONST_2$ are some constants specifying a minimal distance between the unconnected nodes and the upper bound on the difference between the total edge lengths of the real and model networks, respectively.

Output: The model FRC network.

for *i = 1 to* N^3 **do**
  for *j = all neighbors of node [i]* **do**
    if *(NodeIndex [i] == free) and (NodeIndex [j] == free)* **then**
      setline(NodeIndex [i], NodeIndex [j], random (EdgeTarget))
    end
  end
end

RepeatLabel :

$\epsilon = 0$;

for *i = 1 to* N^3 **do**
  OffsetVector = (0,0,0);
  for *j = 1 to* N^3 **do**
    // Function nodes() indicates connective relations between nodes
    if *nodes (NodeIndex [i], NodeIndex [j]) are connected* **then**
      // Function move() returns offset of the Node [i]
      OffsetVector = OffsetVector + move(node with NodeIndex [i], (EdgeReal(NodeIndex [i], NodeIndex [j]) - EdgeTarget(NodeIndex[i], NodeIndex[j])) / 2)
    end
    if *nodes (NodeIndex [i], NodeIndex [j]) are not connected and EdgeReal(NodeIndex [i], NodeIndex [j])* $< CONST_1$ **then**
      OffsetVector = OffsetVector + move(node with NodeIndex [i], (EdgeReal(NodeIndex [i], NodeIndex [j]) - $CONST_1$) / 2)
    end
  end
  $\epsilon = \epsilon$ + length(OffsetVector);
end
if $\epsilon > CONST_2$ **then**
  goto *RepeatLabel*
end

2.3. Implementation of the algorithm

The algorithm was written in C++ and compiled with MSVS2012. Network graph generation was performed on a Windows 10 workstation with 16 Gbytes of RAM and Intel Xeon CPUs ($E3-1241\ v3\ @\ 3.5\ GHz$). The network with 1330 nodes was generated in 114 sec. It required 740 iterations which resulted in the relative error ϵ of the edge lengths displacement reduction to 0.1. The computational time scales linearly with the order of the network graph. The source code is available upon request to the first author.

3. Examples of networks generated according to specified characteristics

The network graph for the real FRC network generated using the above algorithm is shown in Figure 2 A. The degree- and length distributions of the model network are shown in Figure 4 A-B) and are comparable to the real image-based FRC network data. The convergence of the algorithm in terms of the edge lengths displacement ϵt as a function of the number of iterations required to get the length correct is shown in Figure 2 B.

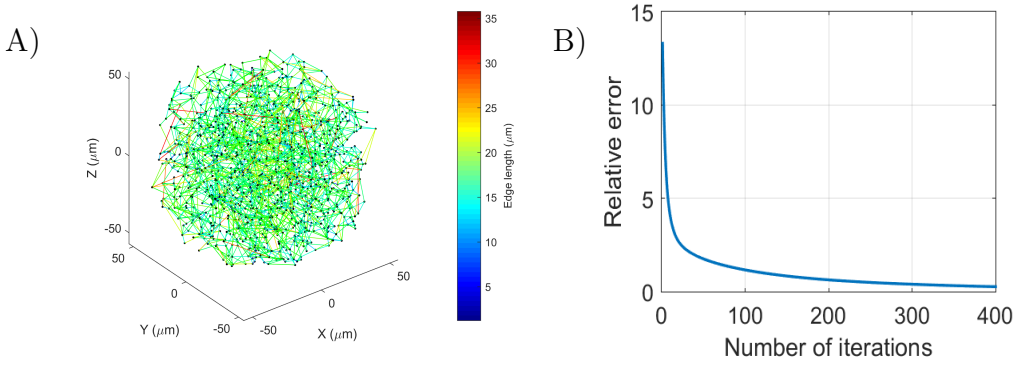

Figure 2: Performance of the algorithm A) The model FRC network. The number of nodes is 1330, the number of edges is 2736. The network statistics is shown in Figure 4 $A-B$). The colorbar represents the edge lengths. B) The convergence of the algorithm in terms of the relative edge lengths displacement error ϵ.

The algorithm was validated by generating other types of model networks that might be relevant under various pathophysiological conditions [18], e.g., the scale-free network with a power law- and the network following a uniform

degree distribution, respectively, as shown in Figure 4 C-D) and E-F). The scale-free network is set to follow the degree distribution $P(k) \sim 2^{8-k},\ k \in [2, 8]$. The network with a uniform degree distribution is given by the pdf $P(k) \sim 1/7,\ k \in [2, 8]$. The scale-free and the uniform degree distribution networks generated by the algorithm are shown in Figure 3 A-B). One can see in increase in the abundance of the short edges in the scale-free network versus the uniform degree distribution network.

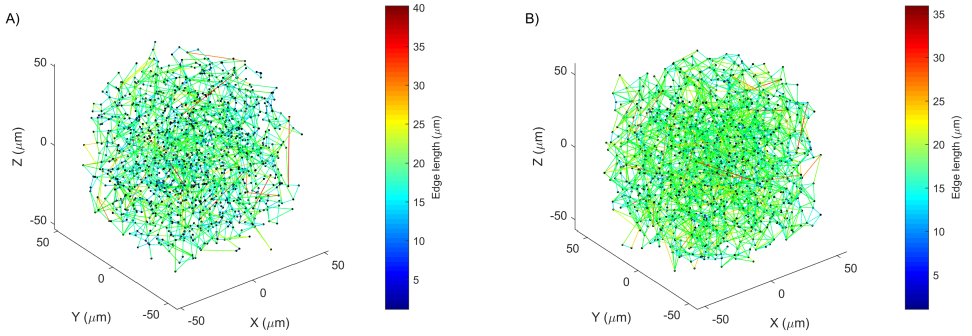

Figure 3: The FRC networks corresponding to scale-free A) and the uniform degree B) distribution generated using the same mean nodal degree and the real data distribution of the edge length. The network statistics are shown in Figure 4 C-D and E-F). The colorbars represent the edge lengths.

The edge length distribution for the generated three networks are shown in Figure 5 A-C). The difference of about 25% in the mean value of the edge lengths of the model network versus the real data (see Figure 1 A) is due to a relatively small size of the constructed FRC network. A ten-fold increase in the number of nodes reduces the difference from the real data average length to practically zero. At the moment there are no other algorithms available for comparing the quality of capturing a real FRC network features for the developed algorithm.

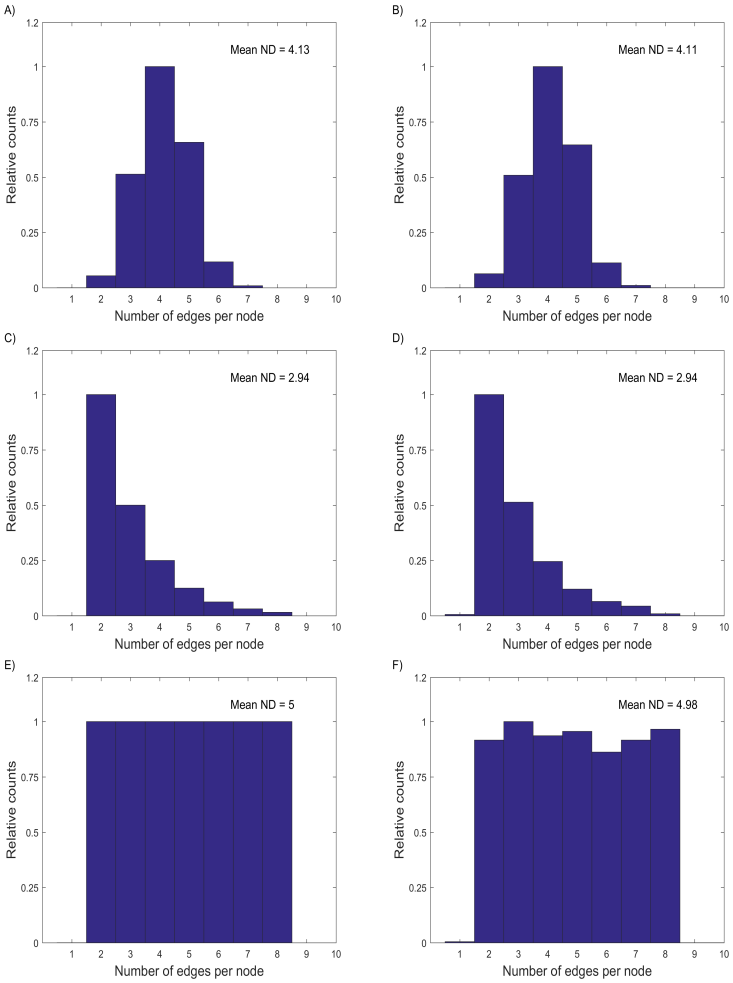

Figure 4: Characteristics of target (left column, A,C,E) and model (algorithm generated) approximation networks (right column, B,D,F): number of edges per node (node degree), ND is the mean number of links per node. $A-B$) Real FRC network data model distribution of edges per node and the model approximation. $C-D$) Target network of a Scale-free type with a power law distribution of the number of links per node and the model approximation; $E-F$) target network with a Uniform distribution of edges per node and the model approximation. Normalized histograms are shown.

4. Application to study the fluid flow through lymph node conduits

4.1. The Flow Model

A steady-state flow solver was developed in MATLAB® to investigate the overall resistance and permeability of the network. The momentum balance

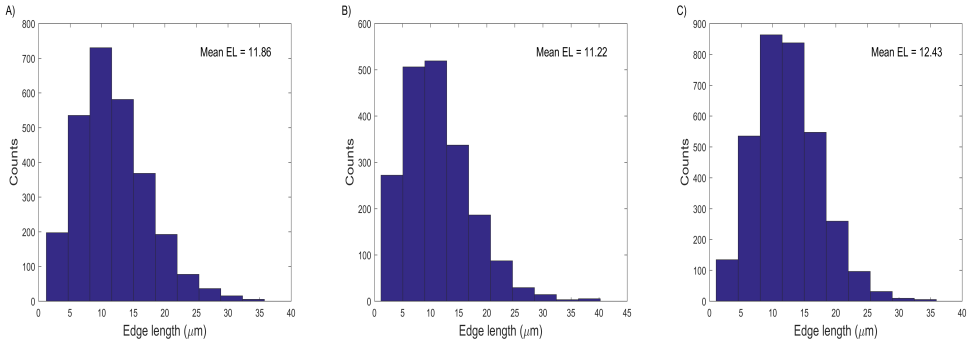

Figure 5: Characteristics of the model approximation of the real data and ideal target networks: edge length distribution, Mean EL is the mean edge length of the networks. A). The model approximation of the real data FRC network. The model approximation of B) the Scale-free network and C) the network with a Uniform distribution of edges per node. EL stands for the edge lengths. The median values are 11.1, 10.2 and 11.9 μm for the different target networks, respectively.

for every 1D segment consisted of a linear relation between flow, Q, and pressure drop along each segment, Δp, with local pipe resistance, R_p, as the proportionality constant. Mass conservation was imposed on all the nodes in the network. The initial mesh was approximately cuboid, but nodes near the boundaries did not lie in a plane, which would be convenient for imposing boundary conditions. Hence, points within two mean element lengths of the two boundaries normal to x were made co-planar in the $y-z$ plane and a pressure drop of 500Pa was then prescribed in the x-direction (Figure 6) as boundary conditions. It should be noted that this might lead to some edges lying in the boundary, which results in zero flow for those edges and will affect the edge length distribution slightly. However, this effect was found to be insignificant. A system matrix was built and static condensation was applied to reduce the system and solve for only pressure p. The code was vectorised to improve performance while a direct solver was used for problems up to 200k nodes and a stabilised biconjugate gradient method was employed for larger problems. All cases were executed on a standard macbook pro (2.9 GHz Intel Core i7, 8Gb 1600 MHz DDR3). In the flow studies presented the radii of all channels were assumed to have a constant value of 1μm, while a viscosity of 1.5cP was chosen (unless stated otherwise). The velocity profile in the channels was approximated as a Hagen-Poiseuille pipe flow. The inflow and outflow are tested to be equal for all simulations suggesting

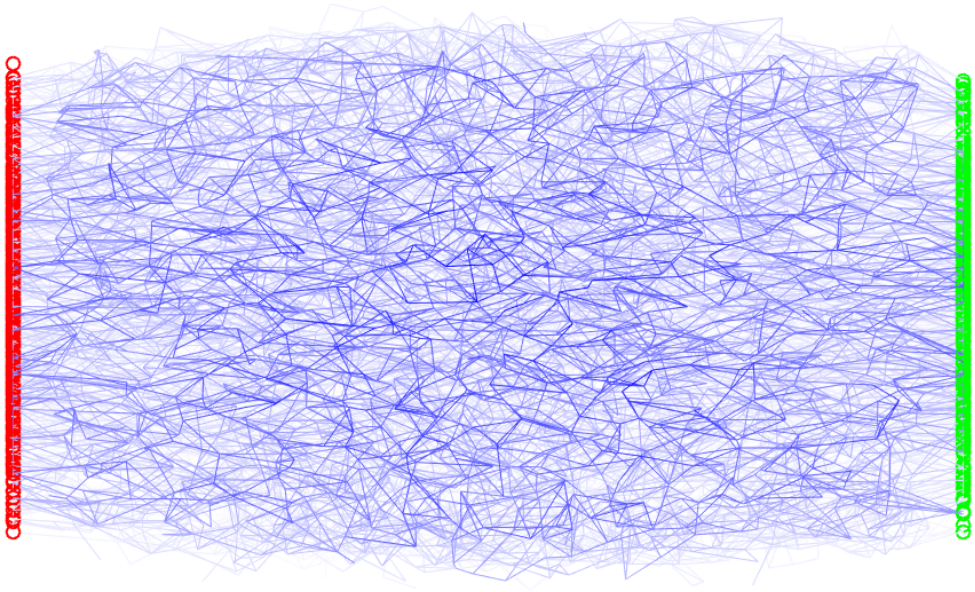

Figure 6: The 3D flow domain with the pipes shown in blue. A pressure of 500Pa is prescribed in the red nodes and 0Pa is prescribed in the green nodes.

a perfect conservation of mass. A network of 24519 edges and 12161 nodes was considered for the flow studies. The inflow boundary consisted of 495 nodes and the outlet consisted of 443 nodes. A zero flow was observed in 4% of the edges, caused by the generation of the boundaries.

4.2. Results

Similarity between the microscale behaviour of the individual pipes and the macroscale behaviours of the network can be seen from the pressure gradient in Figure 7. Homogenisation theory would suggest a linear pressure gradient across the domain, a slight deviation from this can be observed at the boundaries of the network. This is highlighted by the cyan cubic line fitted through the pressure-distance graph. It can be hypothesised that this is due to long pipes spanning large sections of the network. This hypothesis seems justified through the red cubic fit in Figure 7, where a small decreased deviation from linearity can be achieved by removing edges whose length exceeds twice the mean.

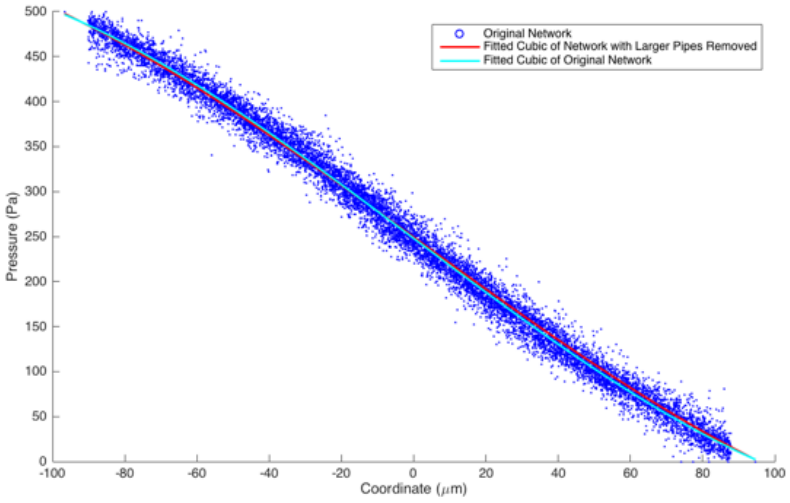

Figure 7: Pressure per node against its coordinate in the direction of the prescribed pressure gradient. Note the deviation from the linearity near the boundaries. A cubic is fitted and can be compared to a cubic fitted to the network with larger pipes removed. Note the reduced inflection.

Through flow simulations in other directions, the network was also found to be reasonably isotropic with intrinsic permeabilities of 0.0034, 0.0033 and 0.0033 μm^2 in the x, y and z directions, respectively, for a pipe radius of 1μm. Swartz and Fleury [33] note the use of Carmen-Kozeny correlations in estimating the permeability of tissues. The relation given is as follows with κ being the permeability; ϵ, the void volume fraction; r_H, the hydraulic radius and b, the Kozeny factor - in this case 8:

$$\kappa = \frac{\epsilon r_H^2}{b} \tag{1}$$

This relationship gives an estimated permeability of 0.0168 μm^2. Indicating factors other than porosity and hydraulic radius play a role in the permeability of such networks. From the constitutive law it is known that for a universal pipe radius the permeability will rise quartically with pipe radius. A range of values from $1.5cP$ to $2.2cP$ were found for lymph viscosity in literature [33] also channel radii in the range between 200nm and 3μm have been observed [26]. Table 1 shows the apparent velocities found for the network

at the extremes of these ranges for pipe radius and viscosity. The apparent velocity is the total flow-rate divided by the cross-sectional area bounding the domain. If the network is imagined within a rectangular cuboid of tissue the apparent velocity is the velocity fluid would appear to have as it seeped through the tissue. This illustrates the significance of pipe radius on the resistance in the network as was expected from the Hagen-Poiseuille profile.

	case 1	case 2	case 3	case 4
Pipe Radius (μm)	0.2	3	1	1
Viscosity (cP)	1.5	1.5	1.5	2
Apparent Velocity(μms^{-1})	480.0	9.480×10^{-3}	5.926	4.040

Table 1: Apparent velocities, i.e. the observed velocity of fluid travelling through a cuboid of tissue containing the network, for extremes of observed values of viscosity and pipe radius

Although the results presented in Table 1 gives some insight, the radial value of all pipes in the network is typically not constant, but distributed across a defined range. This distribution can have a large effect on the resistance of the network. To investigate this further, normal distributions truncated between the bounds $200nm$ and $3\mu m$ with three different means, i.e. 0.9, 1.6 and 2.1 and a variety of standard deviations, were generated. Each pipe was given a radius with a different value drawn from a distribution. This process was repeated a hundred times for each distribution. Shown in Figure 8 is the effect of the distribution on the mean permeability with error bars of length twice the standard deviation. As can be seen the nature of the distribution has a profound effect on the permeability. However, overlap exists between the values found computationally for permeability and those found experimentally within LNs; which range from 10^2 to 10^{-2} μm^2 [7]. Future work should consider the sensitivity of these type of network problems not only to the radii used, but also their probability distribution.

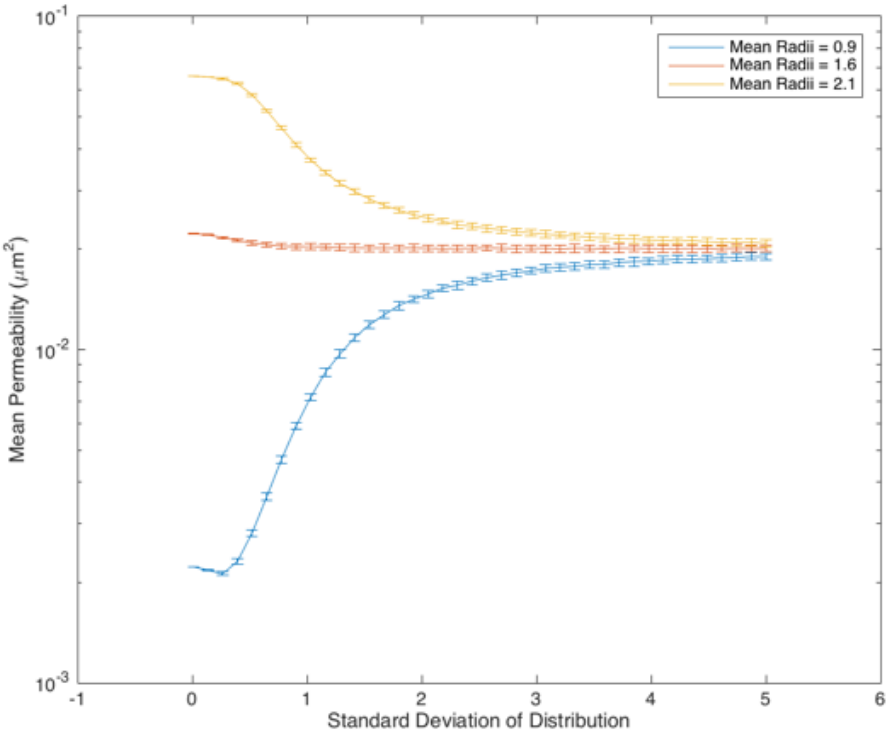

Figure 8: Effect of randomly drawing from widening distributions of radii. Each case was run 100 times and the mean permeability plotted, with error bars at twice the standard deviation.

5. Discussion and future work

We present a computational method to model the geometry of the FRC network. It differs from the vascular network image-based reconstruction approaches as it develops the parameterized geometric model using the real statistics of the nodal degrees and the edges length distributions. Therefore, it can be used to generate various networks to study the impact of the topological properties on the transport and scaffold function of the FRC/conduit network of the LN.

The constructed FRC network model has been used to analyze the fluid flow through the network. It is the first study in which fundamental characteristics of the conduit system such as the dependence of permeability on

the network parameters have been examined. A first observation is that the pressure gradient is approximately linear, which suggests homogeneity of the artificially generated network. Calculated permeability values show the network is also isotropic. A range of typical pipe radii and viscosity were found in the literature, the effect of which on the apparent velocity in the network is quantified and shows a large variability. Finally, a large set of networks is generated for various mean values for the pipe radii, which are then randomly perturbed using a truncated normal distribution with a given STD. These calculations show a significant effect on the permeability and the trends found through this approach will be quite valuable for a further analysis of different networks with varying stochastic properties.

This is a first study in which (1) a computational algorithm for the generation of complex FRC network models (relevant for the LN conduit system) from real data has been proposed and (2) the characteristics of the fluid flow through the network has been explored. The results provide a firm basis for further analysis of this complex information distribution system in LNs under various conditions ranging from its destruction in the course of infections (such as HIV) to remodelling in response to inflammatory stimuli. Understanding the properties of the FRC network is essential for a rational engineering of artificial LNs and the identification of the criteria for therapeutic control of its restoration. Indeed, the FRCs in the LN have been recently shown to directly regulate various components of immune cell function ranging from activation to suppression of T-lymphocytes [1]. Many persistent human infections such as HIV, hepatitis C virus are characterized by collagen deposition and fibrosis. Both processes leading to the reduction of the LN and liver function are the consequences of alterations in the performance of FRCs. The FRC mediated regulation of T cell immunity should depend on the presence of various signaling molecules including those delivered by the lymph flow via the conduit system. Understanding of the information flow through the conduit system in normal conditions and during infections will allow researchers to better determine the impact of specific drugs and medication via a mechanistic modelling of the pharmacokinetics in lymphoid organs. Another area of great interest to quantitative studies of the organization in LN vascular networks, including the blood vascular system, and their role in the performance of lymphoid organs is biomaterials engineering. It has been pointed out that organs of broad interest where its architectural, cellular, and molecular complexity has prevented progress in ex vivo engineering are the secondary lymphoid organs and so far, no immune organ

has been developed with an ability to control the rate of immune reaction through tunable design parameter [25]. The authors engineered a B cell follicle organoid made of nanocomposite biomaterials, which recapitulates the anatomical micro-environment of a lymphoid tissue. The major component of the organoid was the extracellular matrix. Obviously, our ability to synthesize the conduit network according to its role in the real LN is an important step in rational engineering of artificial LNs and identification of the criteria for therapeutic control of its restoration. The micro-scale regulation of multiple extracellular/intracellular molecular dynamics in such a complicated tissue as LNs is still largely unclear. Mathematical models of LN structures will serve as a key rational tool for understanding and translating the design principles of the immune system into biomaterials- or 3D printing-based artificial immune organs.

6. Acknowledgments

The research was funded by the Russian Science Foundation (Grant 14-31-00024).

7. Bibliography

[1] Brown, F.D., Turley, S.J., 2015. Fibroblastic reticular cells: organization and regulation of the T lymphocyte life cycle. J Immunol. 194(4), 1389-94.

[2] Bui, A., Sutalo, I.D., Manasseh, R., Liffman, K., 2009. Dynamics of pulsatile flow in fractal models of vascular branching networks. Med Biol Eng Comput. 47, 763-772.

[3] Bui, A.V., Manasseh, R., Liffman, K., Sutalo, I.D., 2010. Development of optimized vascular fractal tree models using level set distance function. Med Eng Phys. 32, 790-794.

[4] Chapman, B.E., Berty, H.P., Schulthies, S.L., 2015. Automated generation of directed graphs from vascular segmentations. J Biomed Inform. 56, 395-405.

[5] Cohen, I.R., 2007. Real and artificial immune systems: computing the state of the body. Nature Reviews Immunology. 7, 569-574.

[6] Cupedo, T., Stroock, A., Coles, M., 2012. Application of tissue engineering to the immune system: development of artificial lymph nodes. Front. Immun. 3: 343.

[7] Cooper, L.J., Heppell, J.P., Clough, G.F., Ganapathisubramani, B., Roose, T., 2016. An Image-Based Model of Fluid Flow Through Lymph Nodes. Bull Math Biol. 78(1), 52-61.

[8] Danilov, A., Ivanov, Y., Pryamonosov, R., Vassilevski, Y., 2015. Methods of graph network reconstruction in personalized medicine. Int J Numer Method Biomed Eng. e02754, 1-21.

[9] Dasgupta, D., (Ed.), 1999. Artificial Immune Systems and Their Applications. University of Arizona, Springer-Verlag Berlin Heidelberg. ISBN 3-540-64390-7.

[10] Kelch, I. D., Bogle, G., Sands, G. B., Phillips, A. R. J., LeGrice, I. J., Rod Dunbar, P., 2015. Organ-wide 3D-imaging and topological analysis of the continuous microvascular network in a murine lymph node. Scientific Reports. 5, 16534.

[11] Gretz, J.E., Kaldjian, E.P., Anderson, A.O., Shaw, S., 1996. Sophisticated strategies for information encounter in the lymph node: the reticular network as a conduit of soluble information and a highway for cell traffic. J Immunol. 157(2), 495-9.

[12] Gretz, J.E., Norbury, C.C., Anderson, A.O., Proudfoot, A.E., Shaw, S., 2000. Lymph-borne chemokines and other low molecular weight molecules reach high endothelial venules via specialized conduits while a functional barrier limits access to the lymphocyte microenvironments in lymph node cortex. J Exp Med. 192(10), 1425-40.

[13] Jafarnejad, M., Woodruff, M.C., Zawieja, D.C., Carroll, M.C., Moore J.E., 2015. Modeling Lymph Flow and Fluid Exchange with Blood Vessels in Lymph Nodes. Lymphatic research and biology. 13, 234-247.

[14] Zeng, M., Haase, A.T., Schacker, T.W., 2012. Lymphoid tissue structure and HIV-1 infection: life or death for T cells. Trends in Immunology. 33(6), 306-314.

[15] Kislitsyn, A., Savinkov, R., Novkovic, M., Onder, L., Bocharov, G., 2015. Computational Approach to 3D Modeling of the Lymph Node Geometry. Communication. 3(2), 222-234.

[16] Kobourov, S.G., 2012. Spring Embedders and Force Directed Graph Drawing Algorithms. arXiv:1201.3011v1 [cs.CG].

[17] Chai, Q., Onder, L., Scandella, E., Gil-Cruz, C., Perez-Shibayama, C., Cupovic, J., Danuser, R., Sparwasser, T., Luther, S.A., Thiel, V., Rlicke, T., Stein, J.V., Hehlgans, T., Ludewig, B. 2013. Maturation of lymph node fibroblastic reticular cells from myofibroblastic precursors is critical for antiviral immunity. Immunity. 38(5), 1013-24.

[18] Novkovic, M., Onder, L., Cupovic, J., Abe, J., Bomze, D., Cremasco, V., Scandella, E., Stein, J.V., Bocharov, G., Turley, S.J., Ludewig, B., 2016. Topological Small-World Organization of the Fibroblastic Reticular Cell Network Determines Lymph Node Functionality. PLoS Biol. (submitted)

[19] Kumar, V., Scandella, E., Danuser, R., Onder, L., Nitschké, M., Fukui, Y., Halin, C., Ludewig, B., Stein, J.V., 2010. Contextual analysis of immunological response through whole-organ fluorescent imaging. Blood. 115(23), 4725-4733.

[20] Onder, L., Narang, P., Scandella, E., Chai, Q., Iolyeva, M., Hoorweg, K., Halin, C., Richie, E., Kaye, P., Westermann, J., Cupedo, T., Coles, M., Ludewig, B., 2012. IL-7 producing stromal cells are critical for lymph node remodeling. Blood. 120(24), 4675-4683.

[21] Margaris, K.N., Black, R.A., 2014. Modelling the lymphatic system: challenges and opportunities. J R Soc Interface. 9(69), 601-612.

[22] Mayer, J., Swoger, J., Ozga, A.J., Stein, J.V., Sharpe, J., 2012. Quantitative Measurements in 3-Dimensional Datasets of Mouse Lymph Nodes Resolve Organ-Wide Functional Dependencies. Computational and Mathematical Methods in Medicine. vol. 2012, Article ID 128431, 1-8.

[23] McDougall, S.R., Anderson, A.R., Chaplain, M.A., Sherratt, J.A., 2002 Mathematical modelling of flow through vascular networks: implications for tumour-induced angiogenesis and chemotherapy strategies. Bull Math Biol. 64(4), 673-702.

[24] Munn, L.L., Padera, T.P., 2014. Imaging the lymphatic system. Microvascular Research. 96, 55-63.

[25] Purwada, A., Jaiswal, M.K., Ahn, H., Nojima, T., Kitamura, D., Gaharwar, A.K., Cerchietti, L., Singh, A., 2015. Ex vivo engineered immune organoids for controlled germinal center reactions. Biomaterials. 63, 24-34.

[26] Delves, P., Martin, S., Burton, D., Roitt, I., 2011. Roitt's Essential Immunology. Somerset: Wiley. 239

[27] Roozendaal, R., Mebius, R.E., Kraal, G., 2008. The conduit system of the lymph node. Int Immunol. 20(12), 1483-1487.

[28] Schreiner, W., Neumann, F., Neumann, M., End, A., Roedler, S.M., Aharinejad, S., 1995. The influence of optimization target selection on the structure of arterial tree models generated by constrained constructive optimization. J Gen Physiol. 106, 583-599 .

[29] Scianna, M., Bell, C.G., Preziosi, L., 2013. A review of mathematical models for the formation of vascular networks. J Theor Biol. 333, 174-209.

[30] Sixt, M., Kanazawa, N., Selg, M., Samson, T., Roos, G., Reinhardt, D.P., Pabst, R., Lutz, M.B., Sorokin, L., 2005. The conduit system transports soluble antigens from the afferent lymph to resident dendritic cells in the T cell area of the lymph node. Immunity. 22(1), 19-29.

[31] Soudja, S.M., Henri, S., Mello, M., Chasson, L., Mas, A., Wehbe, M., Auphan-Anezin, N., Leserman, L., Van den Eynde, B., Schmitt-Verhulst, A.M., 2011. Disrupted Lymph Node and Splenic Stroma in Mice with Induced Inflammatory Melanomas Is Associated with Impaired Recruitment of T and Dendritic Cells. PLoS ONE 6(7): e22639.

[32] Woodruff, M.C., Herndon, C.N., Heesters, B.A., Carroll, M.C., 2013. Contextual analysis of immunological response through whole-organ fluorescent imaging. Lymphat Res Biol. 11(3), 121-127.

[33] Swartz, M.A., Fleury, M.E., 2007. Interstitial flow and its effects on soft tissue. Annu. Rev. Biomed. Eng. 9. 229-256.